

# Size-controllable synthesis of Fe<sub>3</sub>O<sub>4</sub> nanoparticles through oxidation–precipitation method as heterogeneous Fenton catalyst

Dong Wan, Wenbing Li,<sup>a)</sup> Guanghua Wang, and Xiaobi Wei  
*School of Chemistry and Chemical Engineering, Wuhan University of Science and Technology,  
 Wuhan 430081, China*

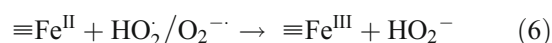
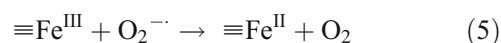
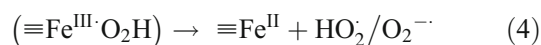
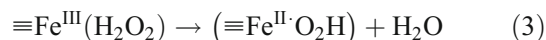
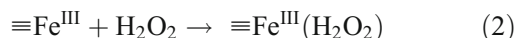
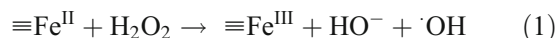
(Received 10 May 2016; accepted 18 July 2016)

The particle size of Fe<sub>3</sub>O<sub>4</sub> nanoparticles is controlled using a simple oxidation–precipitation method without any surfactant. The structure, morphology and physical properties of the synthesized Fe<sub>3</sub>O<sub>4</sub> NPs were characterized using x-ray diffraction, scanning electron microscopy, transmission electron microscopy, x-ray photoelectron spectroscopy, Brunauer–Emmett–Teller, and vibrating sample magnetometer. As-prepared magnetite samples exhibited spherical morphology with average diameters of 30, 70, 250, and 600 nm, respectively. Activity of the synthesized Fe<sub>3</sub>O<sub>4</sub> NPs was evaluated for the Fenton-like reaction, using rhodamine B (RhB) as a model molecule. The results showed that catalytic activity increases with the reduced particle size. The significant higher catalytic activity of the fine Fe<sub>3</sub>O<sub>4</sub> NPs mainly originated from the higher specific surface area, due to the increase in exposed active site number and adsorption capacity. The reusability of 30 nm Fe<sub>3</sub>O<sub>4</sub> NPs was also investigated after three successive runs, in which the RhB degradation performances showed a slight difference with the first oxidation cycle. This investigation is of great significance for the promising application of the heterogeneous Fenton catalyst with enhanced activity in the oxidative degradation of organic pollutants.

## I. INTRODUCTION

As one of the important contaminants of water pollution, the refractory organics have harmful effects on human beings and environment. Since refractory organic pollutants are highly hazardous and suspicious carcinogens, the stringent water quality regulations are imposed and wastewater containing these chemicals must be treated accordingly. Recently, various technologies including biological degradation, physical adsorption and chemical oxidation have been developed to remove the aqueous pollutants. Among these methods, advanced oxidation processes, heterogeneous Fenton process with the capability of exploiting the high reactivity of hydroxyl radicals (·OH) in driving oxidation, emerged a promising technology for the degradation of refractory organic pollutants.<sup>1,2</sup> Various heterogeneous catalysts including iron minerals,<sup>3</sup> zero-valent iron,<sup>4</sup> soils,<sup>5</sup> and carbon materials<sup>6</sup> have been prepared and tested for the Fenton-like oxidation of model pollutants and practical wastewaters to find the new catalytic materials with high activity and stability. Among these materials, magnetite (Fe<sub>3</sub>O<sub>4</sub>) has received much more attention due to its low cost, easy separation, environment-friendly property, strong adsorption capacity, and

enhanced stability.<sup>7,8</sup> Since Fe<sub>3</sub>O<sub>4</sub> nanoparticles (NPs) were found to possess intrinsic peroxidase-like activity,<sup>9</sup> magnetite has been widely explored for the applications in the degradation of various refractory organics such as phenol,<sup>10</sup> pentachlorophenol,<sup>11</sup> *p*-nitrophenol,<sup>12</sup> 2,4-dichlorophenol<sup>13</sup> and dye pollutants.<sup>14</sup> The catalytic mechanism for the activation of H<sub>2</sub>O<sub>2</sub> by Fe<sub>3</sub>O<sub>4</sub> NPs as the heterogeneous Fenton catalyst is shown in Eqs. (1)–(6).<sup>11,14</sup>



The unique crystal structure of Fe<sub>3</sub>O<sub>4</sub> allows the Fe species to be reversibly oxidized and reduced while keeping the same structure, which makes the magnetite to be an excellent catalyst for Fenton-like processes. However, several reports demonstrated that the H<sub>2</sub>O<sub>2</sub>-activating ability of Fe<sub>3</sub>O<sub>4</sub> NPs was not so strong for the

Contributing Editor: Edson Roberto Leite

<sup>a)</sup>Address all correspondence to this author.

e-mail: liwenbing@wust.edu.cn

DOI: 10.1557/jmr.2016.285

removal of refractory organic pollutants from practical wastewaters.<sup>14,15</sup> Furthermore, with a proper control of crystallinity and structure of the Fe<sub>3</sub>O<sub>4</sub> NPs, the functional performance can be strongly improved.

It is well accepted that the particle size of Fe<sub>3</sub>O<sub>4</sub> NPs has a strong effect on their intrinsic properties.<sup>16–18</sup> The particle size of Fe<sub>3</sub>O<sub>4</sub> NPs is generally controlled by the synthesis method. As far, a wide variety of methods to synthesize Fe<sub>3</sub>O<sub>4</sub> NPs have been reported, including hydrothermal method,<sup>19</sup> thermal decomposition,<sup>20</sup> sol–gel method,<sup>21</sup> and chemical precipitation.<sup>22</sup> In practical industrial application, as well as large scale production, the chemical precipitation is considered to be the simplest, most efficient, and economic pathway to obtain magnetic particles. However, there has been few attempts to achieve size-controlled synthesis of Fe<sub>3</sub>O<sub>4</sub> NPs through a simple and economic pathway. Moreover, little is known about the effects of particle sizes in Fenton-like catalytic activity of Fe<sub>3</sub>O<sub>4</sub> NPs.

Herein, we described the size-controllable synthesis of Fe<sub>3</sub>O<sub>4</sub> NPs under a simple and efficient oxidation–precipitation procedure without any surfactant. Using this method, the concentration, pH and the ratio of Fe<sup>2+</sup>/Fe<sup>3+</sup> could be exactly controlled, which might be responsible for the formation of different sizes of Fe<sub>3</sub>O<sub>4</sub> NPs.<sup>23–25</sup> As we known, rhodamine B (RhB) is one of the most commonly used xanthenes dyes for the textile industry. The RhB can well dissolve in water or organic solvent with many toxic effects such as irritation to the skin, eyes, and respiratory tracts. Even more serious, RhB was believed to be carcinogenic, which made it be banned from using in foods and cosmetics. However, the RhB is still extensively used in dyeing and staining processes.<sup>26</sup> Therefore, an efficient treatment of effluents containing RhB is essential before their final discharge into the aquatic environment. Besides, RhB has been selected as a model dyeing pollutant in numerous researches on Fenton reaction.<sup>14,27–30</sup> In this study, the synthesized Fe<sub>3</sub>O<sub>4</sub> NPs of various sizes were used as heterogeneous Fenton catalysts for adsorbing and degrading RhB in the presence of H<sub>2</sub>O<sub>2</sub>. The physical and chemical characterization of Fe<sub>3</sub>O<sub>4</sub> was performed and the structural effects on their Fenton-like catalytic activity were investigated, which is of great importance for obtaining a profound understanding of catalytic processes, as well as for improving the catalytic properties of materials.

## II. EXPERIMENTAL SECTION

### A. Synthesis of the Fe<sub>3</sub>O<sub>4</sub> NPs

The Fe<sub>3</sub>O<sub>4</sub> NPs of various sizes were synthesized by oxidation–precipitation method. Ferrous sulfate (FeSO<sub>4</sub>) was used as iron salts, and sodium nitrate (NaNO<sub>3</sub>) was used as the oxidizing agent. All chemical reagents were of analytical grade and used as received. In all

experiments, distilled water was used for preparing the solutions. In a typical procedure for the fabrication of Fe<sub>3</sub>O<sub>4</sub> NPs with diameters of approximately 600 nm (denoted as sample d), 3.2 g of NaOH was dissolved in 100 mL distilled water after using N<sub>2</sub> to lustrate oxygen in it for 20 min. 100 mL of 0.5 M FeSO<sub>4</sub> aqueous solution was added dropwise into the flask under stirring and N<sub>2</sub> flow. The solution was subsequently placed into a 95 °C water bath. Afterward, 50 mL of 0.5 M NaNO<sub>3</sub> aqueous solution was added dropwise (10 mL/min) into the suspension and the reaction was kept for 4 h. Vigorous stirring and stable N<sub>2</sub> flow were kept during the entire experiment. After cooled to room temperature, the formed Fe<sub>3</sub>O<sub>4</sub> NPs were collected under the assistance of a magnet and washed five times with distilled water and absolute ethanol under ultrasonication, and then dried in a vacuum oven at 100 °C for 12 h.

When NaNO<sub>3</sub> was increased 3-fold and reaction time was reduced by half, we added the NaOH aqueous solution dropwise into the mixed solution of FeSO<sub>4</sub> and NaNO<sub>3</sub> in the above procedures while keeping other parameters unchanged, 250 nm Fe<sub>3</sub>O<sub>4</sub> (denoted as sample c) NPs were obtained. Similarly, when FeSO<sub>4</sub> aqueous solution was added dropwise into the mixed solution of NaOH and NaNO<sub>3</sub> in the procedures of fabrication of 250 nm Fe<sub>3</sub>O<sub>4</sub> NPs without changing other parameters, 70 nm Fe<sub>3</sub>O<sub>4</sub> NPs (denoted as sample b) were synthesized. 30 nm Fe<sub>3</sub>O<sub>4</sub> NPs (denoted as sample a) were obtained similarly with the 70 nm Fe<sub>3</sub>O<sub>4</sub> NPs when the concentration of reactants was reduced 3-fold. All the products were stored in desiccator under ambient temperature for further experiments.

### B. Characterization

The structure and morphology of the Fe<sub>3</sub>O<sub>4</sub> samples were characterized by x-ray powder diffractometer (XRD; Rigaku D/max-RB, Tokyo, Japan) with Cu K<sub>α</sub> radiation, scanning electron microscopy (SEM; FEI Nova400, FEI Company, Brno, Czech Republic) and transmission electron microscopy (TEM; JEOL JEM-100CXII, Tokyo, Japan). High resolution TEM images were obtained by using JEOL JEM-2100F microscope operated at an acceleration voltage of 100 kV. Magnetic characterization of the samples was performed using a JDAW-2000D vibrating sample magnetometer (Yingpu Corp., Hangzhou, China) at room temperature. N<sub>2</sub> adsorption–desorption isotherms of the samples were recorded on an ASAP 2020-M micropore physisorption analyzer (Micromeritics, Atlanta, Georgia). Specific surface areas were calculated by the Brunauer–Emmett–Teller (BET) method. The bulk ratio between Fe<sup>II</sup> and Fe<sup>III</sup> in the Fe<sub>3</sub>O<sub>4</sub> was determined by 1,10-phenanthroline spectrophotometric method after the samples were dissolved in acidic media at 60 °C for

48 h under a nitrogen atmosphere.<sup>5,11</sup> The surface ratio of Fe<sup>II</sup>/Fe<sup>III</sup> on the Fe<sub>3</sub>O<sub>4</sub> surface was analyzed by x-ray photoelectron spectroscopy (XPS; VG Multilab 2000, Thermo Fisher Scientific, Waltham, Massachusetts). Curve fittings were achieved with the XPSPeak 4.1 program using the Fe 2*p* binding energies region for the analysis.

### C. Sorption experiments

To determine the adsorption performance of the obtained Fe<sub>3</sub>O<sub>4</sub> NPs toward organic pollutant, sorption isotherm experiment was carried out at room temperature (25 °C) in the dark. The solid samples were mixed with aqueous solutions of RhB at different initial concentrations, stirring 12 h to ensure the adsorption equilibrium. Before analysis, the suspensions were magnetically separated and the clear water phase was decanted. Then the equilibrium concentrations of RhB in the aqueous phase were measured and sorbed concentrations were calculated according to:

$$q_e = \frac{(C_i - C_e)V}{M_s}, \quad (7)$$

where,  $q_e$  (mg/g),  $C_i$  (mg/L),  $C_e$  (mg/L),  $M_s$  (g), and  $V$  (L) are the sorbed RhB concentration, initial concentration, equilibrium concentration, sorbent dosage, and volume of the solution, respectively.

### D. Fenton-like catalytic activity test

The Fenton-like catalytic activity test was performed under room temperature (25 °C) in a 250 mL glass reactor (containing 100 mL of reaction solution) continuously stirred using RhB (Shanghai Zhanyun Chemical Co., Ltd., Shanghai, China) as reactant and H<sub>2</sub>O<sub>2</sub> as oxidant. The reaction pH value was adjusted to 3.0, the optimum pH for the typical Fenton process, before the oxidation.<sup>3,10</sup> Before reaction, the suspension containing Fe<sub>3</sub>O<sub>4</sub> (1 g/L) and RhB (40 mg/L) was stirred for 2 h to achieve adsorption equilibrium. The degradation reaction was initiated when H<sub>2</sub>O<sub>2</sub> (50 mM) was added to the solution. During all the oxidation reactions, 5 mL aliquots were withdrawn and clarified quickly by a strong outer permanent magnet at selected time intervals. The aqueous phase was sampled for analysis. The solid catalyst separated from the aqueous phase was rinsed by 5 mL distilled water for three times. The rinsed liquid was mixed for analysis. The residual RhB amount is the sum of that in the aqueous and solid phase. The concentration of RhB was analyzed by UV–vis spectroscopy (Ultrospec 3300 pro, GE Healthcare Bio-Sciences China Ltd., Shanghai, China) at a wave length of 554 nm.<sup>28</sup> The chemical oxygen demand (COD) was measured by the dichromate method. At the end of the catalytic test, the concentration of iron leaching in the solution was measured by the

1,10-phenanthroline spectrophotometric method. All experimental runs were performed in the dark.

## III. RESULTS AND DISCUSSION

### A. Characterization of the synthesized Fe<sub>3</sub>O<sub>4</sub> NPs

X-ray diffraction (XRD) was carried out to identify the structures and crystallinity of the synthesized Fe<sub>3</sub>O<sub>4</sub> NPs. As shown in Fig. 1, all of the obtained products show peaks at 18.3, 30.1, 35.5, 43.1, 53.5, 57.0, and 62.6°, which can be indexed to the reflections from crystal planes (111), (220), (311), (400), (422), (511), and (440) of the cubic phase of Fe<sub>3</sub>O<sub>4</sub> according to the standard JCPDS data (card no. 01–1111).<sup>31</sup> The absence of any unidentified peaks in Fig. 1 indicates that the synthesized NPs are pure and crystalline. Additionally, there was a difference in XRD peak intensity among the XRD patterns of the four Fe<sub>3</sub>O<sub>4</sub> NPs samples. The application of Scherrer equation to the (311) reflection peak indicated

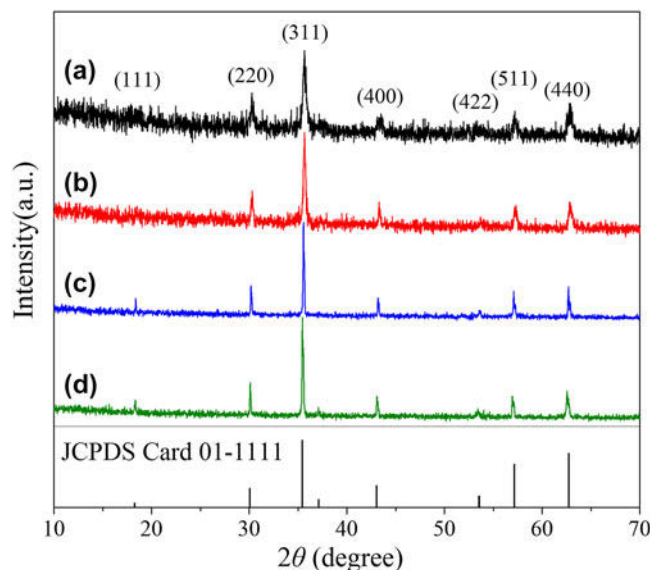


FIG. 1. XRD patterns of the synthesized Fe<sub>3</sub>O<sub>4</sub> NPs: (a) 30 nm, (b) 70 nm, (c) 250 nm, and (d) 600 nm.

TABLE I. Comparison of the structural characteristics of the synthesized Fe<sub>3</sub>O<sub>4</sub> NPs.

Sample	$d_{311}$ (nm)	Average size (nm)	$S_{\text{BET}}^{\text{a}}$ (m <sup>2</sup> /g)	$M_s$ (emu/g)	$H_c$ (Oe)	$q_m^{\text{b}}$ (mg/g)	Fe <sup>II</sup> /Fe <sup>III</sup> ratio <sup>c</sup>
(a)	21.7	30	42.64	80.9	63	34.64	0.51 ± 0.2
(b)	39.5	70	39.51	82.5	79	27.79	0.49 ± 0.2
(c)	60.8	250	6.39	84.2	81	5.44	0.53 ± 0.2
(d)	80.5	600	2.86	88.3	118	3.49	0.55 ± 0.2

<sup>a</sup> $S_{\text{BET}}$  is the specific surface area evaluated using the BET model.

<sup>b</sup> $q_m$  is the monolayer adsorption capacity evaluated using the Langmuir model.

<sup>c</sup>Bulk ratio between Fe<sup>II</sup> and Fe<sup>III</sup> in Fe<sub>3</sub>O<sub>4</sub>.

that the crystal sizes were 21.7, 39.5, 60.8, and 80.5 nm for the four Fe<sub>3</sub>O<sub>4</sub> NPs samples, as listed in Table I.

The size and morphology of the four Fe<sub>3</sub>O<sub>4</sub> NPs samples were further studied with SEM and TEM. As can be seen from Fig. 2, the four Fe<sub>3</sub>O<sub>4</sub> NPs samples

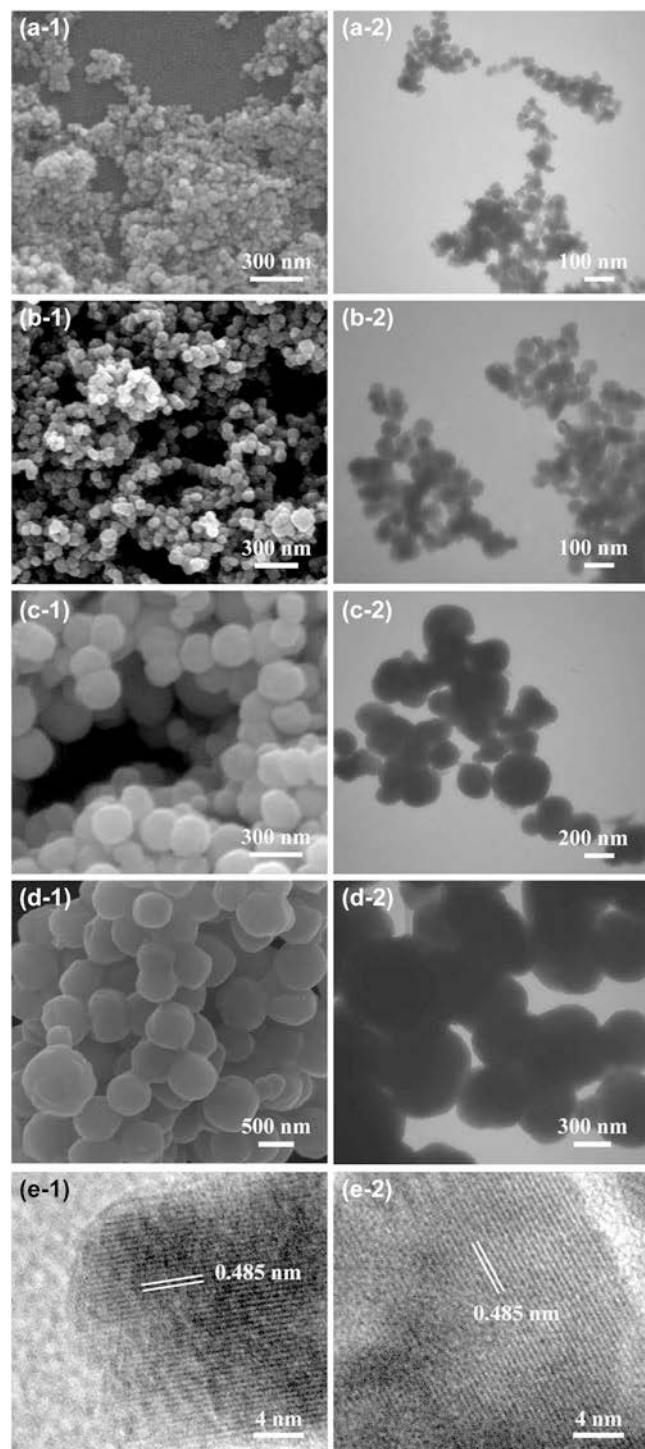
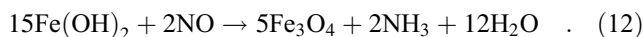
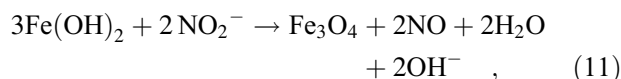
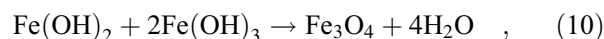
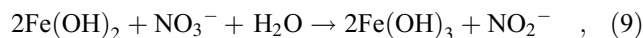
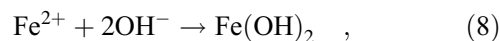


FIG. 2. SEM and TEM images of the synthesized Fe<sub>3</sub>O<sub>4</sub> NPs: (a-1, a-2) 30 nm, (b-1, b-2) 70 nm, (c-1, c-2) 250 nm, and (d-1, d-2) 600 nm, and HR-TEM images of 30 nm Fe<sub>3</sub>O<sub>4</sub> NPs (e-1, e-2).

exhibit spherical morphologies with average particle sizes of approximately 30, 70, 250, and 600 nm, respectively, which are much larger than the crystal size obtained from XRD analysis. The main reason is that the Fe<sub>3</sub>O<sub>4</sub> NPs were the results of secondary growth of crystal grain. The crystal sizes obtained from XRD results represent the sizes of Fe<sub>3</sub>O<sub>4</sub> crystal grains, while the average particle sizes observed from SEM and TEM show the sizes of Fe<sub>3</sub>O<sub>4</sub> NPs. This may be due to the synthesis method of Fe<sub>3</sub>O<sub>4</sub> NPs.<sup>32</sup> As reported, the formation of Fe<sub>3</sub>O<sub>4</sub> follows the nucleation-growth mechanism through oxidation–precipitation method. The nucleation of magnetite particles occurs when the molar ratio of Fe(OH)<sub>2</sub>/Fe(OH)<sub>3</sub> becomes close to 1:2, which is the characteristic value for the magnetite structure. Then the core of Fe<sub>3</sub>O<sub>4</sub> begins to grow up.<sup>32</sup> Therefore, the sizes of the product were strongly depend on reaction conditions such as reaction time, molar ratio of FeSO<sub>4</sub> and oxidizing agent, and the concentration of FeSO<sub>4</sub>, etc. The possible mechanism of formation of Fe<sub>3</sub>O<sub>4</sub> can be described as follows<sup>33</sup>:



In the procedures of fabrication of 600 nm Fe<sub>3</sub>O<sub>4</sub> NPs [Fig. 2(d)], the FeSO<sub>4</sub> was first added into the NaOH solution to form a milk white Fe(OH)<sub>2</sub> suspension. After the addition of NaNO<sub>3</sub>, the suspension gradually turned dark green then black in color, which indicated the formation of Fe<sub>3</sub>O<sub>4</sub>. However, when we increased 3 times of the NaNO<sub>3</sub> dosage and changed the order of adding reagents (adding NaOH into the mixture of FeSO<sub>4</sub> and NaNO<sub>3</sub>), the ratio of ferrous to ferric ions in the metal salt solution was decreased. Thus, the smaller hydroxide particles would be generated readily, resulting in the formation of small Fe<sub>3</sub>O<sub>4</sub> NPs.<sup>23</sup> On the other hand, the reaction time was shortened from 4 to 2 h, which further made the Fe<sub>3</sub>O<sub>4</sub> NPs grow smaller.<sup>24</sup> Thus, the Fe<sub>3</sub>O<sub>4</sub> NPs with smaller dimension [250 nm, Fig. 2(c)] were synthesized using a lower molar ratio of FeSO<sub>4</sub> and oxidizing agent and a shorter growth time. When we further changed the order of adding reagents (adding FeSO<sub>4</sub> into the mixture of NaOH and NaNO<sub>3</sub>), a black precipitate of Fe<sub>3</sub>O<sub>4</sub> NPs was formed in a very short time after mixing the iron salt solution with the base solution, which indicated that

little intermediates were formed prior to the formation of Fe<sub>3</sub>O<sub>4</sub>. This observation demonstrates that the reaction mechanism for the formation of Fe<sub>3</sub>O<sub>4</sub> NPs may be different between the two cases, which may influence the size of Fe<sub>3</sub>O<sub>4</sub> NPs. The formation of Fe<sub>3</sub>O<sub>4</sub> NPs in this case is more likely by the “coprecipitation” reaction,<sup>23</sup> which is supposed to be responsible for the formation of smaller Fe<sub>3</sub>O<sub>4</sub> NPs [70 nm, Fig. 2(b)]. Several papers have reported that the size of the synthesized Fe<sub>3</sub>O<sub>4</sub> NPs increases with the increase of the initial ferric salt concentration.<sup>25,34</sup> In the present study, we have similar results. When the ferric salt concentration was reduced 3-fold, Fe<sup>2+</sup> was kept at a low concentration and could be easily oxidized to Fe<sup>3+</sup>. As a result, more crystal nuclei were generated in the solution, which led to a small particle size [30 nm, Fig. 2(a)]. Moreover, further characterization of crystallinity by HR-TEM was conducted on the 30 nm Fe<sub>3</sub>O<sub>4</sub> NPs. The HR-TEM images shown in Fig. 2(e) demonstrate that highly crystalline Fe<sub>3</sub>O<sub>4</sub> NPs with lattice fringes were formed in the synthesis process, which correspond to (111) plane of Fe<sub>3</sub>O<sub>4</sub> crystal with lattice spacing of 0.485 nm. In general, we are able to prepare satisfying Fe<sub>3</sub>O<sub>4</sub> NPs with controllable sizes by varying the experimental conditions through a simple oxidation–precipitation method with any surfactant.

Magnetic properties of the obtained Fe<sub>3</sub>O<sub>4</sub> NPs were characterized by measuring the applied field dependence of magnetization (Fig. 3). The values of saturation magnetization ( $M_s$ ) and coercivity ( $H_c$ ) read from the magnetization curves are tabulated in Table I. As can be seen, the  $M_s$  and  $H_c$  of the obtained Fe<sub>3</sub>O<sub>4</sub> NPs decreased with the decrease of particle sizes, which may be due to the formation of the magnetically disordered surface as a result of the large surface-to-volume ratio.<sup>35</sup> However, the value of  $M_s$  of the 30 nm Fe<sub>3</sub>O<sub>4</sub> NPs was still as high as 80.9 emu/g, which are found to be 87% of the value of bulk Fe<sub>3</sub>O<sub>4</sub> (93 emu/g).<sup>23</sup> Moreover, room-temperature magnetic

response of the 30 nm Fe<sub>3</sub>O<sub>4</sub> NPs was also examined by an external magnet (Fig. 3 inset). Upon placement of an external magnet beside the sample, the Fe<sub>3</sub>O<sub>4</sub> NPs quickly concentrated on the side, leaving the solution transparent, which demonstrated the excellent magnetic response of the synthesized Fe<sub>3</sub>O<sub>4</sub> NPs to a magnetic field.

Nitrogen adsorption/desorption isotherms of the obtained Fe<sub>3</sub>O<sub>4</sub> NPs showed in Fig. 4 display type II isotherms. The hysteresis area of N<sub>2</sub> adsorption/desorption isotherms suggest the occurrence of capillary condensation and the wide distributions of pores in Fe<sub>3</sub>O<sub>4</sub> NPs. The specific surface areas obtained from N<sub>2</sub> adsorption measurements for the corresponding samples were 42.64, 39.51, 6.39, and 2.86 m<sup>2</sup>/g, respectively, as presented in Table I. Notably, the sample exhibited a smaller crystal size showed larger specific surface area, which was also found in other reports.<sup>14,18</sup> In addition, Fe<sup>II</sup>/Fe<sup>III</sup> ratios of the obtained Fe<sub>3</sub>O<sub>4</sub> NPs were also measured in the bulk by chemical analysis, which are presented in Table I. As can be seen, the Fe<sup>II</sup>/Fe<sup>III</sup> ratios obtained over the synthesized Fe<sub>3</sub>O<sub>4</sub> NPs were close to the theoretical Fe<sup>II</sup>/Fe<sup>III</sup> ratio (0.5) for Fe<sub>3</sub>O<sub>4</sub> materials.

## B. Adsorption isotherm

According to previous studies, the adsorption performance of the catalysts has a strong effect on their catalytic activity.<sup>36</sup> Thus, the adsorption isotherms were carried out to investigate the contaminant sorption on the obtained Fe<sub>3</sub>O<sub>4</sub> NPs (Fig. 5). RhB aqueous solutions with different initial concentrations varying from 5 mg/L to 400 mg/L were used for the adsorption experiment. The experimental isotherm data were fitted to the equations of Langmuir and Freundlich by applying linear regression analysis. On the basis of the statistic analysis, the isotherms can be well described with the Langmuir model which assumed that the single adsorbate binds to a single site on the adsorbent and that all surface sites on

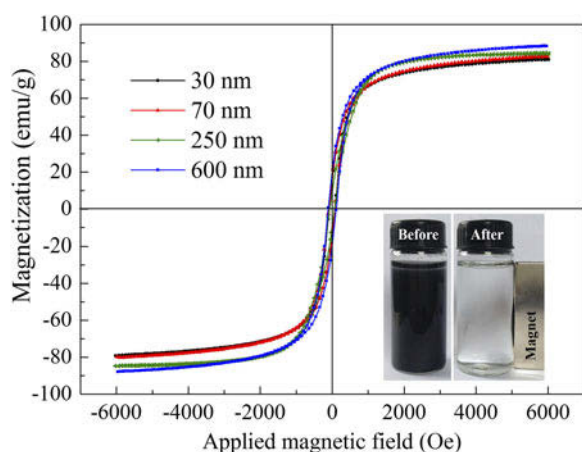


FIG. 3. Hysteresis loop of the synthesized Fe<sub>3</sub>O<sub>4</sub> NPs.

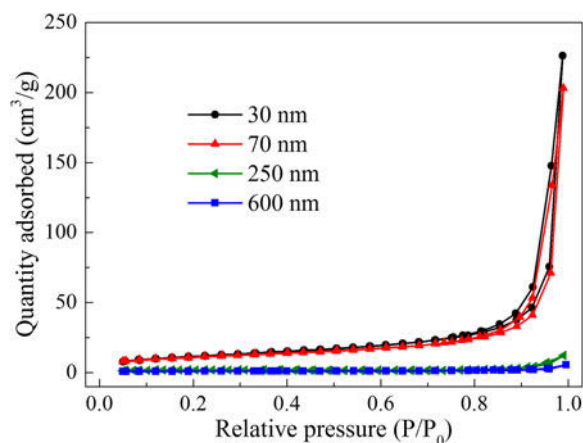


FIG. 4. Nitrogen adsorption/desorption isotherms for the synthesized Fe<sub>3</sub>O<sub>4</sub> NPs.



the adsorbents have the same affinity for the adsorbate and no interactions between the adsorbates. The linear form of the Langmuir equation is given by:

$$q_e = \frac{q_m K_a C_e}{1 + K_a C_e} \quad (13)$$

where  $q_m$  (mg g<sup>-1</sup>) is the monolayer adsorption capacity, and  $K_a$  (L mg<sup>-1</sup>) is the Langmuir constant. The fitted Langmuir equations are  $q_e = 34.64 \times 0.029C_e / (1 + 0.029C_e)$  ( $R^2 = 0.9962$ ),  $q_e = 27.79 \times 0.033C_e / (1 + 0.033C_e)$  ( $R^2 = 0.9849$ ),  $q_e = 5.44 \times 0.027C_e / (1 + 0.027C_e)$  ( $R^2 = 0.9908$ ) and  $q_e = 3.49 \times 0.032C_e / (1 + 0.032C_e)$  ( $R^2 = 0.9898$ ) for the 30, 70, 250, and 600 nm Fe<sub>3</sub>O<sub>4</sub> NPs, respectively. Good correlations imply that the adsorption of RhB on the catalysts is monolayer adsorption. The adsorption capacities of RhB onto the obtained Fe<sub>3</sub>O<sub>4</sub> NPs are listed in Table I. It is obviously shown that the adsorption capacity of Fe<sub>3</sub>O<sub>4</sub> NPs increased with decreasing particle size or increasing specific surface area. As the average particle size decreased to 30 nm, the specific surface area and adsorption capacity reached as high as 42.64 m<sup>2</sup>/g and 34.64 mg/g, respectively, which are almost fifteen and ten times higher than that for the 600 nm Fe<sub>3</sub>O<sub>4</sub> samples.

### C. The catalytic activity of the synthesized Fe<sub>3</sub>O<sub>4</sub> NPs

The catalytic degradation efficiencies of RhB by different sizes of Fe<sub>3</sub>O<sub>4</sub> NPs were shown in Fig. 6(a). The ability of H<sub>2</sub>O<sub>2</sub> for the elimination of RhB without any heterogeneous catalyst was also evaluated. As shown in Fig. 6(a), the RhB conversion is almost negligible in the presence of H<sub>2</sub>O<sub>2</sub> only, which may be due to the low oxidation potential of H<sub>2</sub>O<sub>2</sub> compared with ·OH.<sup>2</sup> When the catalyst was added to the RhB solution, a significant RhB reduction was achieved. The RhB conversion rates of 30, 70, 250, and 600 nm Fe<sub>3</sub>O<sub>4</sub> NPs

were 96.3, 94.3, 73.5, and 49.0% after 300 min, respectively. Many reports have indicated that ·OH could be generated by the reaction between H<sub>2</sub>O<sub>2</sub> and Fe<sub>3</sub>O<sub>4</sub> leading to the degradation of RhB, which has been described in Eqs. (1)–(6). The degradation of RhB in the Fe<sub>3</sub>O<sub>4</sub>/H<sub>2</sub>O<sub>2</sub> system follows the pseudo-first-order kinetics, as given below:

$$-\ln(C_t/C_0) = kt \quad (14)$$

where  $C_0$  and  $C_t$  are the concentrations of RhB at the beginning and time  $t$ , respectively, and  $k$  is the apparent rate constant (min<sup>-1</sup>). The representative plots of  $-\ln(C_t/C_0)$  versus  $t$  are presented in Fig. 6(b) and good correlation coefficients ( $R^2 \sim 0.99$ ) are obtained

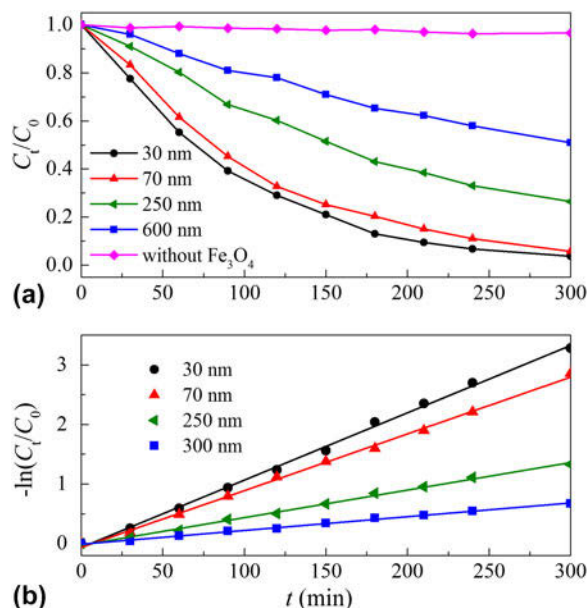


FIG. 6. RhB removal efficiency (a) and pseudo-first-order rate (b) of the synthesized Fe<sub>3</sub>O<sub>4</sub> NPs of different sizes ( $C_0 = 40$  mg/L, [catalyst] = 1 g/L, [H<sub>2</sub>O<sub>2</sub>] = 50 mM,  $T = 25$  °C, pH = 3).

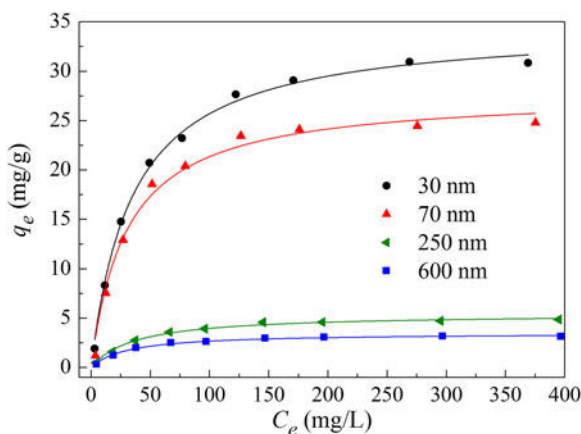


FIG. 5. Isothermal adsorption of RhB on the synthesized Fe<sub>3</sub>O<sub>4</sub> NPs ([adsorbent] = 1 g/L;  $T = 25$  °C).

TABLE II. Selected reaction results and catalyst stability for the RhB degradation ( $C_0 = 40$  mg/L, [catalyst] = 1 g/L, [H<sub>2</sub>O<sub>2</sub>] = 50 mM,  $T = 25$  °C, pH = 3).

Sample	$k$ (min <sup>-1</sup> )	$X_{RhB}^a$ (%)	$X_{COD}^b$ (%)	Fe leaching <sup>c</sup> (mg/L)
(a)-1 <sup>d</sup>	0.0113	96.3	79.5	0.17
(b)	0.0095	94.3	71.6	0.22
(c)	0.0046	73.5	55.8	0.19
(d)	0.0032	49.0	31.6	0.26
(a)-2 <sup>d</sup>	0.0106	95.3	77.2	0.19
(a)-3 <sup>d</sup>	0.0096	93.8	70.5	0.23

<sup>a</sup> $X_{RhB}$  is the RhB conversion after 300 min of reaction.

<sup>b</sup> $X_{COD}$  is the COD abatement after 300 min of reaction.

<sup>c</sup>Fe leaching is the total iron content in the solution at the end of the reaction.

<sup>d</sup>(a)-1, (a)-2 and (a)-3 are the catalysts used for one, two and three successive tests.

in our system. As evident in Fig. 6 and Table II, it is obvious that the 30 nm Fe<sub>3</sub>O<sub>4</sub> NPs exhibited superior catalytic activity in the Fe<sub>3</sub>O<sub>4</sub>/H<sub>2</sub>O<sub>2</sub> process compared with the other sizes of Fe<sub>3</sub>O<sub>4</sub>. The results in Fig. 6, Table I, and Table II then indicated that a greater specific surface area or adsorption capacity was beneficial to the heterogeneous Fenton-like reaction, leading to a high degradation degree of RhB. Figure 7 shows the evolution of the apparent rate constant with the specific surface area. It can be obviously seen that the catalytic activity of Fe<sub>3</sub>O<sub>4</sub> NPs increased with increasing specific surface area. The results indicated that the Fenton-like process in Fe<sub>3</sub>O<sub>4</sub>/H<sub>2</sub>O<sub>2</sub> system was a surface reaction since a larger specific surface area provided more active sites, which lead to more efficient contact with the substrate. Higher content of surface ·OH could be produced over high specific surface area Fe<sub>3</sub>O<sub>4</sub> NPs, enhancing the catalytic oxidation of RhB. On the other hand, the Fe<sub>3</sub>O<sub>4</sub> NPs with smaller particle size could adsorb more RhB molecules on the surface (Table I), which were easily attacked by the generated ·OH, resulting in higher removal efficiency. Similar situations have also been observed in several works that it is the adsorption property of heterogeneous catalyst caused the improvement in the rate of substrate degradation.<sup>7,8,36</sup> It is well accepted that the Fenton-like oxidation by Fe<sub>3</sub>O<sub>4</sub> NPs is controlled by surface mechanism reaction and adsorption of H<sub>2</sub>O<sub>2</sub> or RhB on the surface of magnetite can affect the whole degradation reaction rate.<sup>11</sup> Compared with the 200 or 600 nm Fe<sub>3</sub>O<sub>4</sub> NPs, there are more active sites (such as Fe<sup>II</sup> and Fe<sup>III</sup>) exposed on the surface of 30 nm Fe<sub>3</sub>O<sub>4</sub> NPs, resulting in more active radicals generated according to Eqs. (1)–(4). Meanwhile, more RhB molecules were adsorbed on the surface of 30 nm Fe<sub>3</sub>O<sub>4</sub> NPs. Thus, the reaction between active radicals and RhB on the surface of 30 nm Fe<sub>3</sub>O<sub>4</sub> NPs was accelerated rapidly.

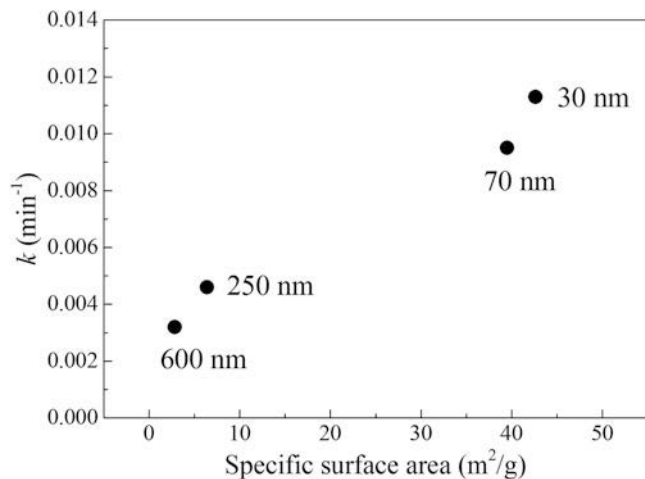


FIG. 7. The relationship between the constant rate and specific surface area of the Fe<sub>3</sub>O<sub>4</sub> NPs of different sizes.

Therefore, the significant higher catalytic activity of the fine Fe<sub>3</sub>O<sub>4</sub> NPs mainly originated from the higher specific surface area, as demonstrated by Fig. 7, due to the increase in exposed active site number and adsorption capacity.

Furthermore, we also examined the contribution of homogeneous Fenton reaction catalyzed by dissolved iron to the whole degradation process. Hence, a special experiment was conducted after the degradation experiment. The solid catalysts were removed from the reaction solution by a Millipore filter (pore size 0.22 μm), then RhB and H<sub>2</sub>O<sub>2</sub> were added to the filtrate. The operation of homogeneous Fenton reaction catalyzed by dissolved iron was similar to that of heterogeneous reaction mentioned in Sec. II. The results showed in Fig. S1 in the supplementary data revealed that the RhB conversion through homogeneous Fenton reaction was below 10% after 300 min. Thus, it indicated that the effect of dissolved iron on the degradation process is limited, which further demonstrated that the whole degradation process of RhB was a surface Fenton-like reaction. Moreover, the dissolved iron concentration was also measured after the reaction (Table II). The Fe leaching did not exceed 0.3 mg/L of each sample, which were negligible.

#### D. Reusability and stability of the synthesized Fe<sub>3</sub>O<sub>4</sub> NPs

To investigate the reusability of the synthesized Fe<sub>3</sub>O<sub>4</sub> NPs as heterogeneous catalysts, the recycling catalysis experiments of the 30 nm Fe<sub>3</sub>O<sub>4</sub> NPs were carried out and the catalytic activity was examined in each cycle. After each recycling, the catalyst was treated by magnetic separation, dried and reused. As shown in Fig. 8 and Table II, only a small decrease in the RhB conversion and COD removal were observed after three successive cycles, with no significant reduction as a whole. XPS was

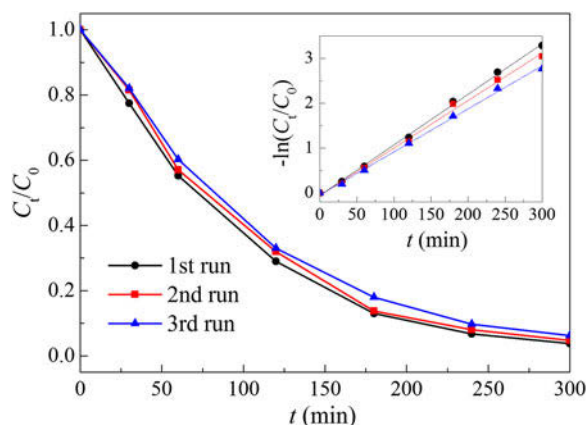


FIG. 8. Effect of recycling the catalyst on the removal of RhB. Inset: fitted by pseudo-first-order rate law ( $C_0 = 40$  mg/L,  $[30 \text{ nm Fe}_3\text{O}_4] = 1$  g/L,  $[\text{H}_2\text{O}_2] = 50$  mM,  $T = 25$  °C,  $\text{pH} = 3$ ).

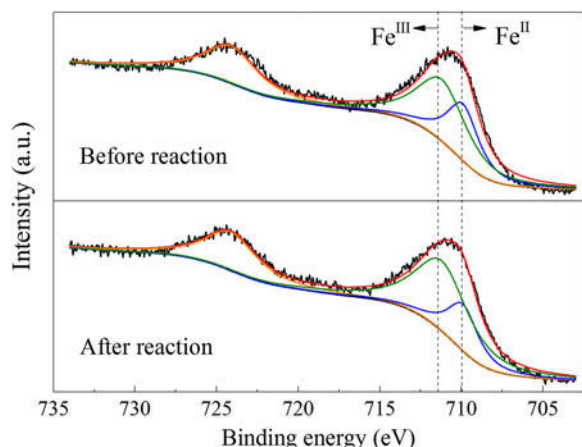


FIG. 9. XPS spectrum of Fe on 30 nm Fe<sub>3</sub>O<sub>4</sub> NPs surface before and after degradation of RhB (Fe 2p line).

used to quantify the changes of surface Fe<sup>II</sup>/Fe<sup>III</sup> ratio. The details of the Fe 2p peaks of the 30 nm Fe<sub>3</sub>O<sub>4</sub> before and after use during the RhB degradation are presented in Fig. 9. The peaks located at about 710.9 and 724.1 eV represented the binding energies of Fe 2p<sub>3/2</sub> and Fe 2p<sub>1/2</sub>, respectively, and the binding energies of 709.9 and 711.2 eV indicated the presence of Fe<sup>II</sup> and Fe<sup>III</sup>, consistent with the literature data for magnetite.<sup>14,37</sup> With the help of peak shape parameters, the Fe 2p<sub>1/2</sub> peak for Fe<sub>3</sub>O<sub>4</sub> was deconvoluted into Fe<sup>II</sup> and Fe<sup>III</sup> component, which is found to be 37.2 and 62.8% of the total iron surface atoms, respectively. For the sample after RhB degradation, the Fe<sup>II</sup> is found to be 27.5% and Fe<sup>III</sup> 72.5%. It is obvious that parts of the Fe<sup>II</sup> in the outermost layer of Fe<sub>3</sub>O<sub>4</sub> are oxidized into Fe<sup>III</sup> during Fenton oxidation reaction, which may lead to the slight decrease in the removal efficiency of RhB between the three successive cycles. However, the RhB conversion and COD removal still remained high (Table II), which indicated that satisfying catalytic activity was maintained after three runs even if the Fe<sub>3</sub>O<sub>4</sub> was observed to slightly dissolve at each cycle (the Fe leaching was 0.17–0.26 mg/L at the end of each test, Table II). In addition, TEM images (Fig. S2) and XRD patterns (Fig. S3) of the Fe<sub>3</sub>O<sub>4</sub> NPs after reaction in the supplementary data showed that the morphology, dimension, and structure of the Fe<sub>3</sub>O<sub>4</sub> NPs remained unchanged, and no clear agglomeration was observed. These results indicate that the synthesized Fe<sub>3</sub>O<sub>4</sub> NPs were stable and exhibited excellent reusability in the catalysis process.

#### IV. CONCLUSIONS

Fe<sub>3</sub>O<sub>4</sub> NPs, which exhibit spherical morphology with different particle sizes (30, 70, 250, and 600 nm), have been successfully fabricated by a simple oxidation–precipitation method without any surfactant. The synthesized Fe<sub>3</sub>O<sub>4</sub> NPs are well-crystallized, as well

as uniform and well-distributed. The Fenton-like catalytic activities of these Fe<sub>3</sub>O<sub>4</sub> NPs vary substantially in the order 30 nm > 70 nm > 250 nm > 600 nm. The significant higher catalytic activity of the fine Fe<sub>3</sub>O<sub>4</sub> NPs mainly originated from the higher specific surface area, due to the increase in exposed active site number and adsorption capacity. Stability studies evidenced satisfying stability of the synthesized Fe<sub>3</sub>O<sub>4</sub> NPs, with limited loss in catalytic activity. This investigation is of particular significance for profound understanding and practical application of heterogeneous Fenton catalysts for the oxidative degradation of organic compounds.

#### ACKNOWLEDGMENTS

This project was supported in part by the Natural Science Foundation of Hubei Province (2014CFB810), Specialized Research Fund for the Doctoral Program of Higher Education of China (20114219110002) and Science and Technology Project (Major) of Jiangxi Province (20152ACG70003).

#### REFERENCES

1. K.H. Kim and S.K. Ihm: Heterogeneous catalytic wet air oxidation of refractory organic pollutants in industrial wastewaters: A review. *J. Hazard. Mater.* **186**(1), 16 (2011).
2. P.V. Nidheesh: Heterogeneous Fenton catalysts for the abatement of organic pollutants from aqueous solution: A review. *RSC Adv.* **5**(51), 40552 (2015).
3. R. Matta, K. Hanna, and S. Chiron: Fenton-like oxidation of 2,4,6-trinitrotoluene using different iron minerals. *Sci. Total Environ.* **385**(1–3), 242 (2007).
4. L. Xu and J. Wang: A heterogeneous Fenton-like system with nanoparticulate zero-valent iron for removal of 4-chloro-3-methyl phenol. *J. Hazard. Mater.* **186**(1), 256 (2011).
5. L. Chen, C. Deng, F. Wu, and N. Deng: Decolorization of the azo dye Orange II in a montmorillonite/H<sub>2</sub>O<sub>2</sub> system. *Desalination* **281**, 306 (2011).
6. L. Gu, N. Zhu, H. Guo, S. Huang, Z. Lou, and H. Yuan: Adsorption and Fenton-like degradation of naphthalene dye intermediate on sewage sludge derived porous carbon. *J. Hazard. Mater.* **246–247**, 145 (2013).
7. S. Song, H. Yang, R. Rao, H. Liu, and A. Zhang: High catalytic activity and selectivity for hydroxylation of benzene to phenol over multi-walled carbon nanotubes supported Fe<sub>3</sub>O<sub>4</sub> catalyst. *Appl. Catal., A* **375**(2), 265 (2010).
8. G.M. Ucoski, F.S. Nunes, G. DeFreitas-Silva, Y.M. Idemori, and S. Nakagaki: Metalloporphyrins immobilized on silica-coated Fe<sub>3</sub>O<sub>4</sub> nanoparticles: Magnetically recoverable catalysts for the oxidation of organic substrates. *Appl. Catal., A* **459**, 121 (2013).
9. L. Gao, J. Zhuang, L. Nie, J. Zhang, Y. Zhang, N. Gu, T. Wang, J. Feng, D. Yang, S. Perrett, and X. Yan: Intrinsic peroxidase-like activity of ferromagnetic nanoparticles. *Nat. Nanotechnol.* **2**(9), 577 (2007).
10. J. Zhang, J. Zhuang, L. Gao, Y. Zhang, N. Gu, J. Feng, D. Yang, J. Zhu, and X. Yan: Decomposing phenol by the hidden talent of ferromagnetic nanoparticles. *Chemosphere* **73**(9), 1524 (2008).
11. X. Xue, K. Hanna, M. Abdelmoula, and N. Deng: Adsorption and oxidation of PCP on the surface of magnetite: Kinetic experiments and spectroscopic investigations. *Appl. Catal., B* **89**(3–4), 432 (2009).



12. S.P. Sun and A.T. Lemley: *p*-Nitrophenol degradation by a heterogeneous Fenton-like reaction on nano-magnetite: Process optimization, kinetics, and degradation pathways. *J. Mol. Catal. A: Chem.* **349**(1–2), 71 (2011).
13. L. Xu and J. Wang: Fenton-like degradation of 2,4-dichlorophenol using Fe<sub>3</sub>O<sub>4</sub> magnetic nanoparticles. *Appl. Catal., B* **123–124**, 117 (2012).
14. N. Wang, L. Zhu, D. Wang, M. Wang, Z. Lin, and H. Tang: Sono-assisted preparation of highly-efficient peroxidase-like Fe<sub>3</sub>O<sub>4</sub> magnetic nanoparticles for catalytic removal of organic pollutants with H<sub>2</sub>O<sub>2</sub>. *Ultrason. Sonochem.* **17**(3), 526 (2010).
15. X. Liang, Z. He, Y. Zhong, W. Tan, H. He, P. Yuan, J. Zhu, and J. Zhang: The effect of transition metal substitution on the catalytic activity of magnetite in heterogeneous Fenton reaction: In interfacial view. *Colloids Surf., A* **435**, 28 (2013).
16. F.F. Peng, Y. Zhang, and N. Gu: Size-dependent peroxidase-like catalytic activity of Fe<sub>3</sub>O<sub>4</sub> nanoparticles. *Chin. Chem. Lett.* **19**(6), 730 (2008).
17. Y.F. Shen, J. Tang, Z.H. Nie, Y.D. Wang, Y. Ren, and L. Zuo: Tailoring size and structural distortion of Fe<sub>3</sub>O<sub>4</sub> nanoparticles for the purification of contaminated water. *Bioresour. Technol.* **100**(18), 4139 (2009).
18. L. Hou, Q. Zhang, F. Jérôme, D. Duprez, H. Zhang, and S. Royer: Shape-controlled nanostructured magnetite-type materials as highly efficient Fenton catalysts. *Appl. Catal., B* **144**, 739 (2014).
19. G. Zhang, F. Qie, J. Hou, S. Luo, L. Luo, X. Sun, and T. Tan: One-pot solvothermal method to prepare functionalized Fe<sub>3</sub>O<sub>4</sub> nanoparticles for bioseparation. *J. Mater. Res.* **27**(7), 1006 (2012).
20. S. Asuha, B. Suyala, X. Siqintana, and S. Zhao: Direct synthesis of Fe<sub>3</sub>O<sub>4</sub> nanopowder by thermal decomposition of Fe-urea complex and its properties. *J. Alloys Compd.* **509**(6), 2870 (2011).
21. A. Prakash, A.V. McCormick, and M.R. Zachariah: Aero-sol–gel synthesis of nanoporous iron-oxide particles: a potential oxidizer for nanoenergetic materials. *Chem. Mater.* **16**(8), 1466 (2004).
22. K. Petcharoen and A. Sirivat: Synthesis and characterization of magnetite nanoparticles via the chemical co-precipitation method. *Mater. Sci. Eng., B* **177**(5), 421 (2012).
23. L. Li, J. Ding, and J. Xue: A facile green approach for synthesizing monodisperse magnetite nanoparticles. *J. Mater. Res.* **25**(5), 810 (2010).
24. A. Yan, X. Liu, G. Qiu, H. Wu, R. Yi, N. Zhang, and J. Xua: Solvothermal synthesis and characterization of size-controlled Fe<sub>3</sub>O<sub>4</sub> nanoparticles. *J. Alloys Compd.* **458**(1–2), 487 (2008).
25. H. Meng, Z. Zhang, F. Zhao, T. Qiu, and J. Yang: Orthogonal optimization design for preparation of Fe<sub>3</sub>O<sub>4</sub> nanoparticles via chemical coprecipitation. *Appl. Surf. Sci.* **280**, 679 (2013).
26. Y. Zhang, W. Shi, D. Feng, H. Ma, Y. Liang, and J. Zuo: Application of rhodamine B thiolactone to fluorescence imaging of Hg<sup>2+</sup> in *Arabidopsis thaliana*. *Sens. Actuators, B* **153**(1), 261 (2011).
27. B. Chai, F. Zou, and W. Chen: Facile synthesis of Ag<sub>3</sub>PO<sub>4</sub>/C<sub>3</sub>N<sub>4</sub> composites with improved visible light photocatalytic activity. *J. Mater. Res.* **30**(8), 1128 (2015).
28. X. Xue, K. Hanna, and N. Deng: Fenton-like oxidation of Rhodamine B in the presence of two types of iron (II, III) oxide. *J. Hazard. Mater.* **166**(1), 407 (2009).
29. P.P. Gan and S.F.Y. Li: Efficient removal of rhodamine B using a rice hull-based silica supported iron catalyst by Fenton-like process. *Chem. Eng. J.* **229**, 351 (2013).
30. X. Wang, Y. Pan, Z. Zhu, and J. Wu: Efficient degradation of rhodamine B using Fe-based metallic glass catalyst by Fenton-like process. *Chemosphere* **117**, 638 (2014).
31. S. Liu, F. Lu, R. Xing, and J.J. Zhu: Structural effects of Fe<sub>3</sub>O<sub>4</sub> nanocrystals on peroxidase-like activity. *Chem. - Eur. J.* **17**(2), 620 (2011).
32. W. Yu, T. Zhang, J. Zhang, X. Qiao, L. Yang, and Y. Liu: The synthesis of octahedral nanoparticles of magnetite. *Mater. Lett.* **60**(24), 2998 (2006).
33. S. Yang, H. He, D. Wu, D. Chen, X. Liang, Z. Qin, M. Fan, J. Zhu, and P. Yuan: Decolorization of methylene blue by heterogeneous Fenton reaction using Fe<sub>3–x</sub>Ti<sub>x</sub>O<sub>4</sub> (0 < x < 0.78) at neutral pH values. *Appl. Catal., B* **89**(3–4), 527 (2009).
34. K. Tao, H. Dou, and K. Sun: Interfacial coprecipitation to prepare magnetite nanoparticles: Concentration and temperature dependence. *Colloids Surf., A* **320**(1–3), 115 (2008).
35. G.F. Goya, T.S. Berquó, F.C. Fonseca, and M.P. Morales: Static and dynamic magnetic properties of spherical magnetite nanoparticles. *J. Appl. Phys.* **94**(5), 3520 (2003).
36. D. Wan, W. Li, G. Wang, K. Chen, L. Lu, and Q. Hu: Adsorption and heterogeneous degradation of rhodamine B on the surface of magnetic bentonite material. *Appl. Surf. Sci.* **349**, 988 (2015).
37. T. Yamashita and P. Hayes: Analysis of XPS spectra of Fe<sup>2+</sup> and Fe<sup>3+</sup> ions in oxide materials. *Appl. Surf. Sci.* **254**(8), 2441 (2008).

### Supplementary Material

To view supplementary material for this article, please visit <http://dx.doi.org/10.1557/jmr.2016.285>.